Probing electron correlation, charge transfer, and Coster-Kronig transitions at the $3d$ and $4d$ thresholds of Nd by resonant inelastic scattering

A. Moewes
Center for Advanced Microstructures and Devices, CAMD at Louisiana State University, Baton Rouge, Louisiana 70803

D. L. Ederer
Physics Department, Tulane University, New Orleans, Louisiana 70118

M. M. Grush and T. A. Callcott
University of Tennessee, Knoxville, Tennessee 37996

(Received 14 July 1998)

Soft x-ray emission near the $3d$-$4f$ and $4d$-$4f$ thresholds of Nd_2O_3 is studied with monochromatic synchrotron radiation excitation. At excitation energies above the M_{IV} threshold, we observe Coster-Kronig enhanced fluorescence from the refill of the $3d$ hole via the $5p$ and $4f$ channel. Fluorescence occurs mainly due to transitions in which charge-transfer provides additional $4f$ electrons. Resonant inelastic scattering dominates the emission process and we observe two energy loss features at 2.3 and 21 eV, which are due to net transitions within the $4f$ shell ($4f^3 \rightarrow 4f^3$) and $5p^6 4f^3 \rightarrow 5p^5 4f^4$, respectively. The emission spectra resulting from excitations at various energies through the $3d$ and $4d$ thresholds were compared and a number of differences were found. Our atomic calculations are in excellent agreement with the experimental results indicating strong localization and a low degree of correlation of the $4f$ electrons. [S0163-1829(99)01707-5]

INTRODUCTION

Lanthanides are characterized by their partly filled $4f$ shell. The combination of the high degree of localization and the low binding energy of the $4f$ electrons has stimulated great interest in these materials. Most studies have focused on photoelectron emission,[1,2] and due to the low $3d$ and $4d$ emission intensity only a few x-ray emission spectroscopy (XES) studies have been carried out so far on lanthanides.[3–5] With the availability of intense x-ray sources, inelastic scattering phenomena have become of great interest, in general,[6,7] and of rare-earth materials in particular. Soft XES has been used to study the degree of hybridization[8] and the role of charge-transfer processes.[9,10] While most previous experiments used electron bombardment or hard x-ray excitation,[11,9,12] only a few XES experiments on lanthanides have been performed using tunable synchrotron radiation. The $3d$-$4f$ threshold has been studied on compounds of Ce (Ref. 3) and Pr (Ref. 13) and at the $4d$-$4f$ threshold of Gd.[4,5] Excitations within the $4f$ shell give rise to energy losses of the exciting radiation in many rare-earth compounds.[14,4] In Ce, however, the energy-loss features cannot be explained by the $4f$ inner-shell excitations. Tanaka and Kofani[15] applied the Anderson impurity model[16] in a theoretical study of LaF_3 and CeF_3. In this localized approach, the hybridization of $4f^0$ and $4f^1\,\underline{L}$ states is included, and the results suggest that the f electrons can sometimes have bandlike and localized character. For PrO_2, the emission at the $3d$-$4f$ threshold is explained within the framework of this model.[13]

We wished to study if a purely atomic model for the emission involving $4f$ electrons is viable, or the alternative approach to the Anderson impurity model. In this paper, we present the first excitation-energy selective study of the $3d$ and $4d$ threshold phenomena in Nd_2O_3. We find that at and below the excitation threshold of the $3d$ electrons, the emission is dominated by inelastic scattering. Our results indicate strong Coster-Kronig decay of the $3d_{3/2}$ hole as well as additional occupancy of the $4f$ level via charge transfer from the oxygen valence band only for the $3d$-$4f$ threshold. Strong inelastic scattering produces energy losses of 2.3 and 21 eV, which are due to $4f$ inner-shell excitations [$4f^3 \rightarrow (4f^3)^*$] and $5p$-$4f$ excitations ($5p^6 4f^3 \rightarrow 5p^5 4f^4$), respectively. The results are explained by our atomic calculations indicating strong localization of the $4f$ electrons and suggesting that correlation effects and hybridization of the $4f$ electrons are weak.

EXPERIMENT

Our emission experiments were performed at Beamline 8.0 of the Advanced Light Source, Lawrence Berkeley Laboratory. This undulator beamline is equipped with a spherical grating monochromator[17] with a maximum resolving power of $E/\Delta E = 10\,000$. The fluorescence end station consists of a Rowland circle grating spectrometer that provides a resolving power of about 300 at 985 eV and about 700 at 130 eV. The incident angle of the *p*-polarized beam was about 15° to the sample normal. The absorption spectrum was taken at Beamline 6.3.2 (Ref. 18) of the Advanced Light Source by measuring the total photoelectron current. The sample was an insulating Nd_2O_3 single crystal. In order to perform the absorption measurement with the sample current technique and avoid charging effects, Nd_2O_3 powder was pressed into an indium foil support. The resolving power for the absorption measurement is 3300.

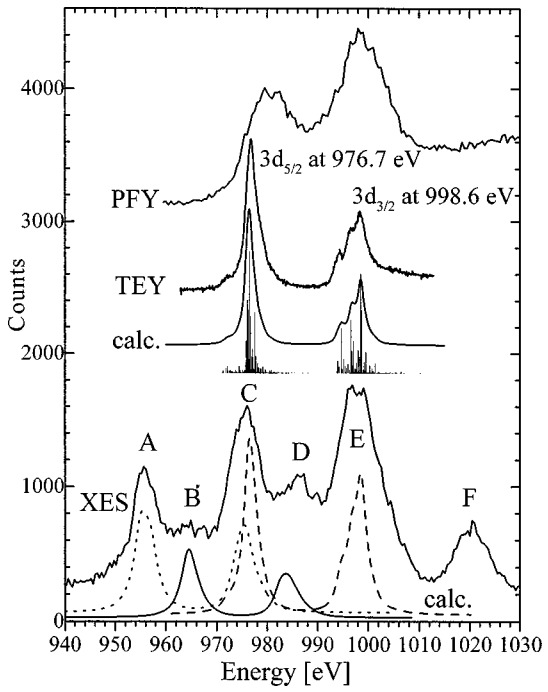

FIG. 1. Soft XES excited above the $3d$-$4f$ threshold, TEY spectrum, PFY of Nd_2O_3, and calculated transitions for atomic Nd in the vicinity of the $3d$-$4f$ threshold.

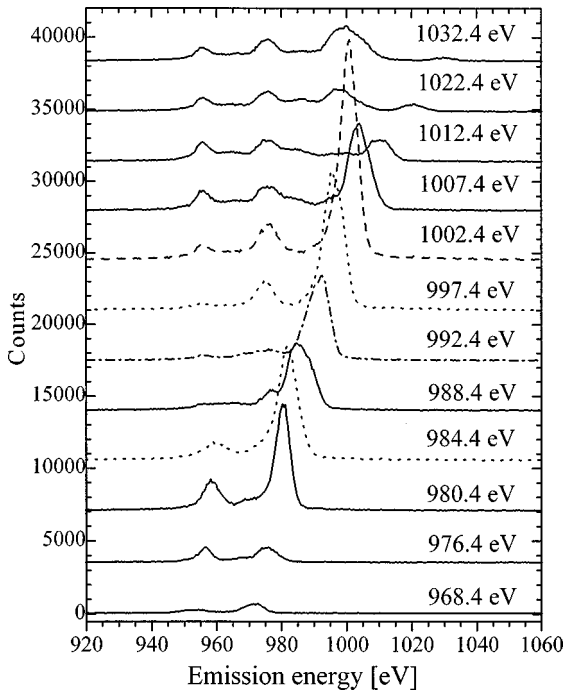

FIG. 2. Soft x-ray emission spectra of Nd_2O_3 excited in the region of the $3d$-$4f$ threshold. The excitation energy for the spectra is given above each spectrum.

RESULTS AND DISCUSSION

In Fig. 1 the XES of Nd_2O_3 above the $3d$-$4f$ threshold is displayed. The excitation energy is 1022.4 eV. Six peaks are resolved and labeled as A–F. To identify the features, we have calculated the atomic transition rates for Nd by using Cowan's code.[19] The scaling factor for the Slater integrals[20] was 80% and the results are shown below the XES spectrum. The calculated spectra in Fig. 1 have been broadened by 3.3 eV full width at half maximum, which is approximately the theoretical resolution of the spectrometer. Transitions between three different electron configurations were calculated, and each one is displayed in a different line style in Fig. 1. All peaks are due to the filling of the $3d$ hole and the assignment is as follows: peak A, $3d^95p^64f^4\ L\ [^6K \text{ or } 3d_{5/2}] \rightarrow 3d^{10}5p^54f^4\ L\ [^6I]$ (dotted line); peaks B and D, $3d^95p^64f^3\ [^3G] \rightarrow 3d^{10}5p^54f^3\ [^3F]$ (dashed line); peaks C and E, $3d^95p^64f^4\ L\ [C{:}\ ^4K_{11/2} \text{ or } 3d_{5/2},\ E{:}\ ^4H_{7/2} \text{ or } 3d_{3/2}] \rightarrow 3d^{10}5p^64f^3\ L\ [^4I_{9/2}]$ (solid line).

The terms corresponding to the strongest transitions between the electron configurations are given in brackets. Both $\mathbf{L}\cdot\mathbf{S}$ and j-j notation will be used for the terms of the configurations in this paper. The quantity L denotes a ligand hole.

In Nd_2O_3 the Nd atom is triply ionized and the electron configuration is $3d^{10}5p^64f^3$ with a $^4I_{9/2}$ ground-state term. The electron configuration for the intermediate state, leading to peaks A, C, and E, has four electrons in the $4f$ shell. Charge-transfer processes provide additional occupancy of the $4f$ level when exciting above the $3d$-absorption threshold. Charge-transfer electrons from the oxygen valence band can shake down to the $4f$ levels from which the $3d$ hole can be filled. This behavior has been observed in other rare-earth materials.[9,14] Our calculations show also that peak C has some contribution from the transitions that lead to peak A (dotted line). Our data are not corrected for self-absorption because of the uncertainty of the relevant cross sections. The amplitudes of peaks C and E are diminished by self-absorption. Peak F is due to an inelastic loss and will be discussed later.

The absorption of Nd_2O_3 in the region of the $3d$ threshold has been measured by detecting the total electron yield (TEY) and the spectrum is displayed in Fig. 1. The features mainly arise from excitations of the $3d^{10}4f^3(^4I_{9/2})$ ground state to the $^4K_{11/2}(3d_{5/2})$ and $^6K_{9/2}$, $^4I_{9/2}$ and $^4H_{7/2}$ $(3d_{3/2})$ terms of the $3d^94f^4$ configuration. The measured spectrum for Nd_2O_3 is well reproduced in detail including the relative peak height by the calculation for atomic Nd^{3+}. This indicates the strong localization of the $4f$ electrons.

Figure 1 also exhibits the measured partial fluorescence yield (PFY) of Nd_2O_3. It represents the total intensity emitted in the detectable range (880–1100 eV) vs photon-excitation energy. Two differences in electron (TEY) and fluorescence yield (PFY) spectra are apparent: The energetic position of the $3d_{5/2}$ is not the same for the two spectra and the peaks are much broader in the fluorescence-yield spectrum. We will discuss this after introducing the next figure.

In Fig. 2 the measured emission spectra for Nd_2O_3 are shown for various excitation energies through the $3d$-$4f$ thresholds. The counting time for each spectrum was 30 min. The current from a gold mesh placed in the beampath monitored the number of incident photons and all spectra are normalized to this signal. Above the $3d_{3/2}$ threshold (998.6 eV) the spectra display the four fluorescence features as discussed above. We note in passing, that some details cannot been seen clearly because of the large number of spectra displayed. This is due to the extended scale used in Fig. 2. The spectrum taken at an excitation energy of 1022.4 eV is the same XES spectrum as displayed in Fig. 1.

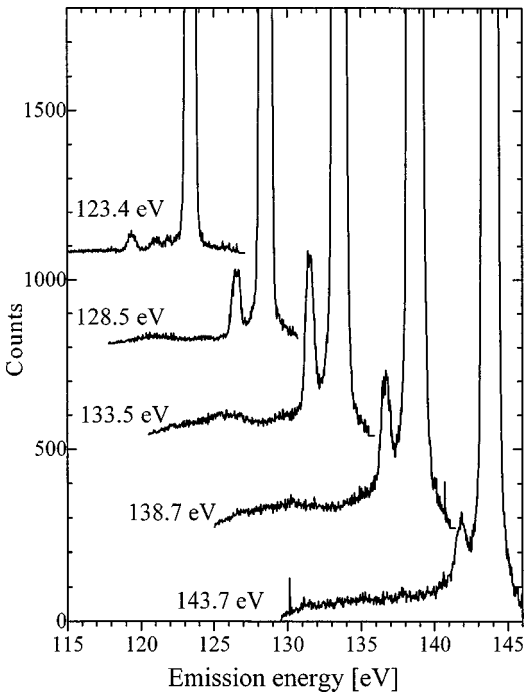

FIG. 3. Soft x-ray emission spectra of Nd_2O_3 in the region through the $4d$-$4f$ threshold. The excitation energy for the spectra is given above each spectrum.

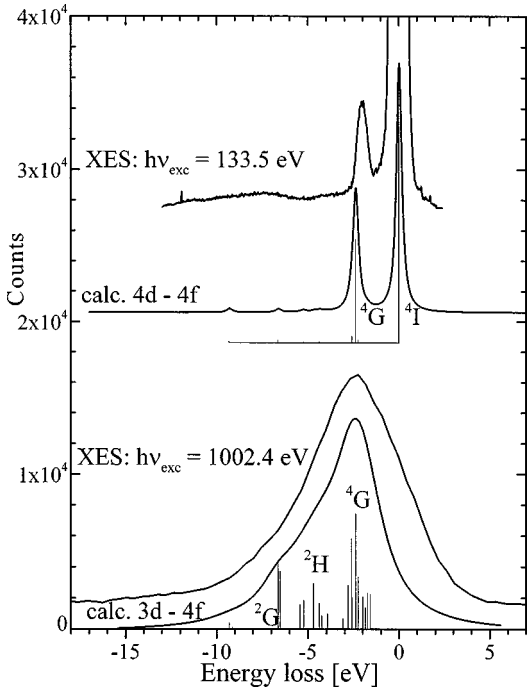

FIG. 4. Energy-loss spectra of Nd_2O_3 for excitation at $3d$-$4f$ threshold, $4d$-$4f$ threshold, and atomic calculations of the loss features. The excitation energy is 1002.4 and 133.5 eV, respectively.

At and below the $3d_{3/2}$ threshold, the fluorescence evolves into inelastic scattering. Comparison of the XES spectra (Fig. 2) and the partial fluorescent yield (Fig. 1) shows that inelastic processes dominate the emission from the sample, especially near the $3d$ absorption thresholds. This behavior has been observed in La as well.[14] The dominating inelastic scattering accounts for the fact that the features in partial fluorescence (PFY in Fig. 1) are broader than in absorption (TEY in Fig. 1), and suggests the intermediate-state lifetime for fluorescence is short compared to the lifetime for total absorption. The inelastic scattering also accounts for the different energetic positions of the peaks in TEY and PFY spectra.

Fluorescence from the decay of the $3d_{5/2}$ hole (peaks *A*, *B*, and *C* in Fig. 1) is observed after creating the $3d_{3/2}$ hole (excitation energies of greater than 998.6 eV). This indicates strong Coster-Kronig decay of the $3d_{3/2}$ hole of the kind: $3d_{3/2} \rightarrow 3d_{5/2}$. When exciting at the $3d_{5/2}$ threshold directly (976.4 eV), only the fluorescence from the decay of the $3d_{5/2}$ is apparent (peaks *A* and *C*).

The soft x-ray emission spectra of Nd_2O_3 excited through the $4d$-$4f$ threshold are shown in Fig. 3. The counting time for each spectrum is 5 min and the data are normalized to the incident number of photons. The peaks representing the elastically scattered radiation are not completely displayed since the count rate for the elastic peak is 30–80 times stronger (depending on the excitation energy) than for the inelastic feature. The spectra show an inelastic feature that is tracking the excitation energy and appears about 2.3 eV below the elastic peak. While intense inelastic and elastic scattering is observed as the photon energy is tuned to the $4d$-$4f$ resonances ($4d^9 4f^4 \rightarrow 4d^{10} 4f^3$), we do not observe fluorescence at excitation energies above the $4d$ shell-ionization threshold due to $4d^9 4f^3 \rightarrow 4d^{10} 4f^2$ transitions. This is expected because the partial cross section to produce a $4d$ hole above threshold is small[1] and the probability is high that the competing Auger processes fill the $4d$ hole. There is no indication of a hole-induced shakedown process such as is apparent at the $3d$-$4f$ threshold.

Near threshold the decay of a core-hole state can be very different from the decay mechanisms at higher energies. Soft x-ray emission and (radiationless) Auger-electron emission can appear as coherent one-step processes also known as the (resonant) Raman effect.[6] In the case of inelastic scattering, the energy loss is assigned to the difference in energy between the initial and the final state, often designated as the ''net transition.'' The inelastic and elastic scattered intensity I is described by the Kramers-Heisenberg (K-H) formula:[21]

$$I(E_{\rm in},E_{\rm out}) \propto \sum_f \left| \sum_m \frac{\langle f|pA|m\rangle\langle m|pA|i\rangle}{E_m - E_i - E_{\rm in} - i\Gamma/2} \right|^2 \times \delta(E_f + E_{\rm out} - E_i - E_{\rm in}). \quad (1)$$

In this equation, pA is the dipole operator while $|i\rangle$ is the initial state of the system with energy E_i, $|m\rangle$ and E_m describe the intermediate state, $|f\rangle$ and E_f describe the final state, and Γ is the lifetime broadening in the intermediate state. $E_{\rm in}$ and $E_{\rm out}$ are the energies of the incident and the emitted photons, respectively.

We have calculated the loss spectra from Eq. (1) using transition rates from the ground state to the intermediate states and back to the final metastable states that were obtained by Cowan's method.[19] We then summed these rates incoherently over the intermediate states of the $nd^9 4f^4$ ($n = 3,4$) configuration. The lifetime broadening Γ was set to 0.5 eV.[22] The result is shown in Fig. 4, where two of the

TABLE I. Initial, intermediate, and final states for inelastic scattering in Nd_2O_3.

	$3d$-$4f$ threshold	$4d$-$4f$ threshold
Initial state	$3d^{10}4f^3(^4I_{9/2})$	$4d^{10}4f^3(^4I_{9/2})$
Intermediate	$3d^9 4f^4$ (main: $^4H_{7/2}$)	$4d^9 4f^4$ (main: $^4H_{7/2}$)
Final state	$3d^{10}4f^3$ (main: ^4G_J, ^2H_J, ^2G_J)	$4d^{10}4f^3$ (main: $^4H_{7/2}$)
Net transition	$3d^{10}4f^3(^4I_{9/2}) \rightarrow 3d^{10}4f^3(^4G_J, {}^2H_J, {}^2G_J)$	$4d^{10}4f_3(^4I_{9/2}) \rightarrow 4d^{10}4f^3(^4G_J)$

measured emission spectra (XES) from Figs. 2 and 3 excited at the $3d$-$4f$ and the $4d$-$4f$ thresholds, respectively, are displayed as energy-loss spectra. The energy loss is derived from the emission spectra by subtracting the energy of the exciting photons from the energy of the emitted photons. The theoretical calculations are shown below the measurements. The initial, intermediate, and final states that were used, as well as the net transition, are shown in Table I.

The loss features correspond to a constant energy loss of about 2.3 eV at both thresholds and are due to $4f$ inner-shell excitations $4f^3 \rightarrow (4f^3)^*$ through the intermediate states of the $nd^9 4f^4$ ($n=3,4$) electron configuration. The calculated $3d$-$4f$ spectrum was broadened by 3.3 eV and the $4d$-$4f$ spectrum by 0.45 eV, respectively. Consequently, the spectra taken at lower energies E ($4d$-$4f$ threshold) provide better resolution ΔE than the ones taken at the high-energy threshold ($3d$-$4f$). The contributions from nondipole transitions (final states ^2G and ^2H) are stronger in the case of the $3d$-$4f$ transitions. This is due to the different overlap of the $3d$ and the $4d$ wave function with the $4f$ wave function.

A second weaker-inelastic feature of about 21 eV energy loss is observed (Fig. 2). It is due to a net transition in which a $5p$ electron is excited into the $4f$ shell ($3d^{10}5p^6 4f^3 \rightarrow 3d^9 5p^6 4f^4 \rightarrow 3d^{10}5p^5 4f^4$). In the absence of $4f$ electrons this process can dominate the emission at the $3d$-$4f$ threshold as has been observed in lanthanum.[14] In the case of the excitation of the $4d$-$4f$ threshold, the inelastic feature due to the $5p$-$4f$ net transition is extremely weak (50 counts).

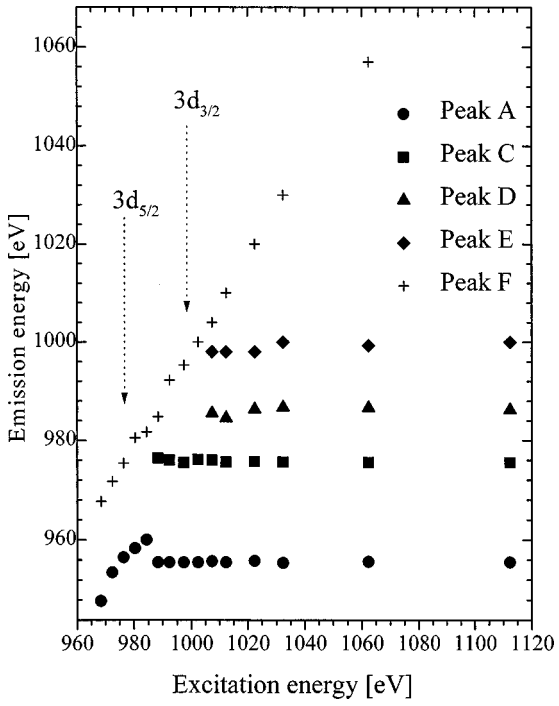

FIG. 5. Emission energy vs excitation energy for the five emission peaks *A*, *C*, *D*, *E*, and *F* in the region of the $3d$-$4f$ threshold. The dotted vertical lines indicate the $3d_{5/2}$ and $3d_{3/2}$ thresholds in the absorption spectrum.

Displaying the emission energy vs excitation energy for the five emission peaks *A*, *C*, *D*, *E*, and *F*, allows one to easily observe the emission change from inelastic scattering to fluorescence as shown in Fig. 5.

At about 10 eV above the $3d_{5/2}$ threshold, the inelastic scattering that leads to the 21 eV energy loss evolves into the fluorescence peak, which has the same intermediate and final state (peak *A*). Peak *C* corresponds to transitions originating from the same electron configuration as peak *A* and, therefore, it begins to fluoresce at the same excitation energy. The onset of the fluorescent decays of the $3d$ hole via the $5p$ channel (peak *D*) and via $4f$ channel (peak *E*) is apparent at the corresponding $3d_{3/2}$ threshold. The inelastic scattering due to $4f$ inner-shell excitations (peak *F*) takes place over a wide energy range and resonates about 8 eV above the $3d_{5/2}$ and even more strongly at the $3d_{3/2}$ threshold (Fig. 2). This inelastic scattering dominates the emission through $3d$ as well as the $4d$ thresholds.

SUMMARY

To summarize, we have used soft x-ray inelastic scattering excited with synchrotron radiation to elucidate the role of $4f$ electrons in recombination processes at the $3d$ and $4d$ thresholds. Emission at the $3d$ threshold is dominated by inelastic scattering and the two observed loss mechanisms at 2.3 and 21 eV are due to the net transitions $4f^3 \rightarrow (4f^3)^*$ and $5p^6 4f^3 \rightarrow 5p^5 4f^4$, respectively. The emission spectra excited above the $3d_{3/2}$ threshold indicate Coster-Kronig decay ($3d_{3/2} \rightarrow 3d_{5/2}$) of the $3d_{3/2}$ hole (peaks *A* and *C* in Fig. 1) as well as strong charge-transfer processes (peaks *A*, *C*, and *E* in Fig. 1).

When comparing the emission spectra excited through the $3d$-$4f$ and the $4d$-$4f$ threshold, we note some aspects that are different: The contribution of nondipole transitions ($^4I \rightarrow {}^2G$, ^2H) to the inelastic scattering is stronger at the $3d$ than at the $4d$ threshold (Fig. 4); only the $3d$-$4f$ spectra exhibit charge-transfer and Coster-Kronig processes; while the main inelastic process at both thresholds is the excitation of the electrons within the $4f$ shell (2.3-eV-energy loss), the $5p$-$4f$ energy loss (21 eV) is not apparent at the $4d$ threshold; and at the $4d$ threshold, radiationless processes such as Auger-electron emission and autoionization suppress fluores-

cence from the decay of the vacancy in the d shell via the $4f$ channel.

Our atomic calculations are in excellent agreement with the experimental results emphasizing the localized character of the $4f$ electrons. While the emission of rare-earth systems with fewer $4f$ electrons, like Ce (Ref. 3) and Pr (Ref. 13) have been discussed in the framework of the Anderson impurity model[16] there is no indication that such effects need to be taken into account in the case of Nd.

ACKNOWLEDGMENTS

This paper was supported by National Science Foundation Grant No. DMR-9017997, the Science Alliance Center for Excellence Grant from the University of Tennessee, and DoE-EPSCor cluster research Grant No. DoE-LEQSF (1993–95)-03. The Advanced Light Source is supported by the office of Basic Energy Sciences, U.S. Department of Energy, under Contract No. DE-AC03-76SF00098.

[1] M. Richter, M. Meyer, M. Pahler, T. Prescher, E. v. Raven, B. Sonntag, and H.-E. Wetzel, Phys. Rev. A **40**, 7007 (1989).
[2] J. A. D. Matthew, J. Electron Spectrosc. Relat. Phenom. **72**, 133 (1995).
[3] S. M. Butorin, D. C. Mancini, J. H. Guo, N. Wassdahl, J. Nordgren, M. Nakazawa, S. Tanaka, T. Uozomi, A. Kotani, Y. Ma, K. E. Myano, B. A. Karlin, and D. K. Suth, Phys. Rev. Lett. **77**, 574 (1996).
[4] A. Moewes, T. Eskildsen, D. L. Ederer, J. Wang, J. McGuire, and T. A. Callcott, Phys. Rev. B **57**, R8059 (1998).
[5] J.-J. Gallet, J.-M. Mariot, C. F. Hague, F. Sirotti, M. Nakazawa, H. Ogasawara, and A. Kotani, Phys. Rev. B **54**, 14 238 (1996).
[6] *Resonant Anomalous X-ray Scattering*, edited by G. Materlik, C. J. Sparks, and K. Fischer (Elsevier, New York, 1994), and references therein.
[7] *Resonant Inelastic Soft X-ray Scattering*, edited by W. Eberhardt, Special issue of Appl. Phys. A: Mater. Sci. Process. **65** (1997).
[8] K. Jouda, S. Tanaka, K. Soda, and O. Aita, J. Phys. Soc. Jpn. **64**, 192 (1995).
[9] M. Okusawa, K. Ichikawa, O. Aita, and K. Tsutsumi, Phys. Rev. B **35**, 478 (1987).
[10] D. R. Mueller, C. W. Clark, D. L. Ederer, J. J. Jia, W. L. O'Brien, Q. Y. Dong, and T. A. Calcott, Phys. Rev. A **52**, 4457 (1995).
[11] T. M. Zimkina, A. S. Shulakov, A. P. Braiko, A. P. Stepanov, and V. A. Fomichev, Fiz. Tverd. Tela (Leningrad) **26**, 1981 (1984) [Sov. Phys. Solid State **26**, 1201 (1984)].
[12] K. Ichikawa, A. Nisawa, and K. Tsutsumi, Phys. Rev. B **34**, 6690 (1986).
[13] S. M. Butorin, L.-C. Duda, J.-H. Guo, N. Wassdahl, J. Nordgren, M. Nakazawa, and A. Kotani, J. Phys.: Condens. Matter **9**, 8155 (1997).
[14] A. Moewes, S. Stadler, R. Winarski, D. L. Ederer, M. M. Grush, and T. A. Calcott, Phys. Rev. B **58**, R15 951 (1998).
[15] S. Tanaka and A. Kotani, J. Phys. Soc. Jpn. **61**, 4212 (1992).
[16] O. Gunnarson and K. Schönhammer, Phys. Rev. B **28**, 4315 (1983).
[17] J. J. Jia, T. A. Calcott, J. Yurkas, A. W. Ellis, F. J. Himpsel, M. G. Samant, G. Stöhr, D. L. Ederer, J. A. Carlisle, E. A. Hudson, L. J. Terminello, D. K. Shuh, and R. C. C. Perera, Rev. Sci. Instrum. **66**, 1394 (1995); **66**, 1394 (1995).
[18] J. H. Underwood, E. M. Gullikson, M. Koike, and P. J. Batson, Proc. SPIE **3113**, 214 (1997).
[19] R. D. Cowan, *The Theory of Atomic Structure and Spectra* (University of California Press, Berkeley, 1981).
[20] H. Ogasawara and A. Kotani, J. Phys. Soc. Jpn. **64**, 1394 (1995).
[21] See, e.g., J. J. Sakurai, *Advanced Quantum Mechanics* (Addison-Wesley, Reading, MA, 1967) Chap. 2; T. Aberg, Phys. Scr. **21**, 495 (1980); J. Tulkki and T. Aberg, J. Phys. B **15**, L435 (1982).
[22] E. J. McGuire, Phys. Rev. A **5**, 1052 (1972).